

# Comparison of electrophysiological properties of two types of pre-sympathetic neurons intermingled in the hypothalamic paraventricular nucleus

Yiming Shen<sup>1</sup>, Seong Kyu Han<sup>2</sup>, Pan Dong Ryu<sup>1,\*</sup>

<sup>1</sup>Department of Veterinary Pharmacology, College of Veterinary Medicine and Research Institute of Veterinary Science, Seoul National University, Seoul 08826, Korea

<sup>2</sup>Department of Oral Physiology, School of Dentistry and Institute of Oral Bioscience, Chonbuk National University, Jeonju 54896, Korea

The hypothalamic paraventricular nucleus (PVN) contains two types of neurons projecting to either the rostral ventrolateral medulla (PVN<sub>RVL</sub>) or the intermediolateral horn (IML) of the spinal cord (PVN<sub>IML</sub>). These two neuron groups are intermingled in the same subdivisions of the PVN and differentially regulate sympathetic outflow. However, electrophysiological evidence supporting such functional differences is largely lacking. Herein, we compared the electrophysiological properties of these neurons by using patch-clamp and retrograde-tracing techniques. Most neurons (>70%) in both groups spontaneously fired in the cell-attached mode. When compared to the PVN<sub>IML</sub> neurons, the PVN<sub>RVL</sub> neurons had a lower firing rate and a more irregular firing pattern ( $p < 0.05$ ). The PVN<sub>RVL</sub> neurons showed smaller resting membrane potential, slower rise and decay times, and greater duration of spontaneous action potentials ( $p < 0.05$ ). The PVN<sub>RVL</sub> neurons received greater inhibitory synaptic inputs (frequency,  $p < 0.05$ ) with a shorter rise time ( $p < 0.05$ ). Taken together, the results indicate that the two pre-sympathetic neurons differ in their intrinsic and extrinsic electrophysiological properties, which may explain the lower firing activity of the PVN<sub>RVL</sub> neurons. The greater inhibitory synaptic inputs to the PVN<sub>RVL</sub> neurons also imply that these neurons have more integrative roles in regulation of sympathetic activity.

**Keywords:** action potential, inhibitory postsynaptic current, patch-clamp techniques, rostral ventrolateral medulla, spinal cord lateral horn

## Introduction

The paraventricular nucleus (PVN) neurons of the hypothalamus have a critical role in integrating autonomic and endocrine functions [36]. The PVN has two major cell types, magnocellular and parvocellular neurons [35]. The magnocellular neurons synthesize vasopressin or oxytocin and project to the posterior pituitary to release these compounds into the bloodstream [12,28]. The parvocellular neurons are composed of neurosecretory and non-secretory neurons. The neurosecretory parvocellular neurons synthesize regulatory hormones and project to the median eminence, where they regulate secretions from the anterior pituitary and collaborate with the hypothalamo-pituitary-adrenocortical axis [31,32]. The non-secretory parvocellular neurons are intermingled in

the dorsal, ventral, and lateral subdivisions of the PVN. These neurons project to autonomic control centers, as well as to the sympathetic and parasympathetic preganglionic neurons in both the medulla and the spinal cord [23,30]

The parvocellular PVN neurons, directly and indirectly, project to the sympathetic preganglionic neurons, hence, are commonly called 'pre-sympathetic neurons'. The pre-sympathetic PVN neurons constitute a heterogeneous population consisting of cells with different physiological and morphological properties that distinguish them from other PVN neuronal types [2,26,34]. These neurons project to the rostral ventrolateral medulla (RVL) in the brain stem (PVN<sub>RVL</sub>) and the intermediolateral horn (IML) in the spinal cord (PVN<sub>IML</sub>), and show immunoreactivity to various hormones and neuropeptides [6,15,20]. The PVN<sub>RVL</sub> and PVN<sub>IML</sub> neurons

Received: 24 Jan. 2018, Revised: 6 Mar. 2018, Accepted: 9 Mar. 2018

\*Corresponding author: Tel: +82-2-880-1254; Fax: +82-2-879-0378; E-mail: [pdryu@snu.ac.kr](mailto:pdryu@snu.ac.kr)

Supplementary data is available at <http://www.vetsci.org> only.

Journal of Veterinary Science · © 2018 The Korean Society of Veterinary Science. All Rights Reserved.

This is an Open Access article distributed under the terms of the Creative Commons Attribution Non-Commercial License (<http://creativecommons.org/licenses/by-nc/4.0>) which permits unrestricted non-commercial use, distribution, and reproduction in any medium, provided the original work is properly cited.

pISSN 1229-845X  
eISSN 1976-555X

overlap, are located largely within the same subdivisions of the PVN [2,26], are involved in the regulation of arterial pressure and the sympathetic nervous system, and connect to peripheral sympathetic nerves from the heart and kidneys [10].

In spite of the similarity of their locations in the PVN, these two groups of neurons are different classical transmitters and neural peptide transmitters [4,15]. Different responses to various environments have been reported in PVN<sub>RVLM</sub> and PVN<sub>IML</sub> neurons. For instance, heat-induced Fos-positive PVN<sub>IML</sub> neurons [8] are double-labeled (activated and nitrergic), but that is rarely the case for PVN<sub>RVLM</sub> neurons [7]. In addition, our laboratory reported that heart failure induced a significant increase in the firing rate of PVN<sub>RVLM</sub> neurons, but not in PVN<sub>IML</sub> neurons [18]. These reports suggest that the two neuron groups are also likely to be different in their excitability, but this question has not been fully addressed yet. In this study, we compared the intrinsic excitability and synaptic inputs of the two neuron groups in rats by using a slice patch-clamp technique combined with retrograde tracing.

## Materials and Methods

### Animals

All experiments were performed in accordance with the guidelines of the Laboratory Animal Care Advisory Committee of Seoul National University (IACUC approval No. SNU-140926-2). Male Sprague-Dawley rats (body weight, 180–200 g; age, 6–7 weeks) were purchased from Orient Bio (Korea) and housed in a temperature-controlled (24°C–26°C) and light-controlled (12:12-h light-dark cycle) room with free access to food and water.

### General experimental protocol

Rats were randomly divided into two groups. A retrograde dye was injected into either the RVLM or IML. After a recovery period of 7 days, brain slices were prepared to record the electrophysiological activity of the labeled neurons [18].

### Retrograde staining

The two groups of pre-sympathetic neurons, PVN<sub>RVLM</sub> and PVN<sub>IML</sub> neurons, were labeled by injecting the retrograde dye FluoSphere-Red (F-8793, red fluorescent; Molecular Probes, USA) into the RVLM or the IML. Under anesthesia induced by intraperitoneal injections of Zoletil (tiletamine [25 mg/kg] and zolazepam [25 mg/kg]) and Rompun (10 mg/kg), the rat skulls were fixed in stereotaxic frames (SF-7; Narishige, Japan), and the injection points were determined by using a rat stereotaxic atlas [18,25]. For RVLM injections, the surface of the skull was exposed by an incision of the skin of the head, after which, a small hole was made with a dental drill at the appropriate injection point (1.40 mm lateral to the midline, 11.50 mm from the bregma, and 7.90 mm below the dorsal surface), and the

FluoSphere-Red dye was injected into the RVLM area [18]. For IML injections, the skin and muscle were incised, exposing the second thoracic vertebra. With a bone cutter, the upper segment of the spinal column was removed, the dura mater was incised, and a glass capillary filled with FluoSphere-Red dye was injected into the area of the IML from the surface of the spinal cord. The injection point was 0.5 mm lateral to the midline and 0.75 mm below the dorsal surface [18]. In both retrograde tracings, 100 nL of fluorescent microsphere dye solution was injected unilaterally with a pneumatic picopump (PV820-G; World Precision Instruments, USA). To verify the RVLM and IML injection sites, serial medulla and spinal cord (T2) slices (100 µm thickness) were examined for all animals. Typical examples of the injection sites in the RVLM and IML are shown in panel C in Supplementary Fig. 1. When the injected dye was not identified at the target sites, the results from that animal were excluded from further analysis.

### Brain slice preparation

After recovery from the dye injection, the rats were rapidly decapitated between 10:00 and 12:00. The brains were placed in ice-cold bicarbonate-buffered cutting artificial cerebrospinal fluid (ACSF) with the following composition (in mM): 210 sucrose, 26 NaHCO<sub>3</sub>, 5 KCl, 1.2 NaH<sub>2</sub>PO<sub>4</sub>, 1.2 CaCl<sub>2</sub>, 2.4 MgCl<sub>2</sub>, and 10 glucose (pH 7.4, 311 mOsmol/kg H<sub>2</sub>O, bubbled with 95% O<sub>2</sub> and 5% CO<sub>2</sub>) [18]. The forebrain was blocked and glued with cyanoacrylate to the chilled stage of a vibratome (Vibratome 1000 plus; Vibratome, USA). Then, coronal slices (300 µm thickness) containing the PVN of the hypothalamus were cut in ice-cold cutting ACSF. All slices were allowed to recover in oxygenated ACSF with a composition (in mM) of 126 NaCl, 26 NaHCO<sub>3</sub>, 5 KCl, 1.2 NaH<sub>2</sub>PO<sub>4</sub>, 2.4 CaCl<sub>2</sub>, 1.2 MgCl<sub>2</sub>, and 10 glucose for at least 1 h in an incubation chamber at 32°C until the recordings were made.

### Electrophysiological recording

The brain slices were transferred to a 0.7 mL volume recording chamber, held submerged, and bathed with ACSF at a rate of 4 to 5 mL/min under continuous bubbling with 95% O<sub>2</sub> and 5% CO<sub>2</sub>. The slices were covered by an O-shape platinum wire with single nylon strands. The labeled PVN neurons were identified at ×40 and ×400 objective magnifications by an upright microscope (BX50; Olympus, Japan) with green fluorescence illumination (BH2-RFL-T3; Olympus). The patch pipettes were pulled from thin-wall borosilicate glass-capillary tubing (PC-10; Narishige). The pipette tip resistance ranged from 2 to 4 MΩ, and the seal resistance was much higher (1 GΩ). The recording pipette was filled with one of two kinds of pipette solutions: 1) a K-gluconate-rich pipette solution containing (in mM) 135 K-gluconate, 5 KCl, 20 HEPES, 0.5 CaCl<sub>2</sub>, 5 EGTA, and 5 ATP-Mg for recording firing activity, spontaneous action potentials, miniature excitatory postsynaptic currents

(mEPSCs), and basic membrane properties, or 2) a KCl-rich pipette solution containing (in mM) 140 KCl, 20 HEPES, 0.5 CaCl<sub>2</sub>, 5 EGTA, and 5 ATP-Mg for the analysis of miniature inhibitory postsynaptic currents (mIPSCs) (pH 7.2 with 3M KOH and an osmolality of 312–313 mOsmol/kg H<sub>2</sub>O). The electrical signals were amplified with an Axopatch 200B (Axon Instruments, USA). An analog-digital converter and pClamp software (ver. 8.0; Axon Instruments) were used to sample the electrical signals at 20 kHz and 10 kHz for mIPSC recording.

The shape of the recorded neuron was traced from the images of a PC monitor connected with the 40X objective magnification microscope (WG; Olympus) by using transparent paper. The size of the traced cell was estimated by determining the area of the image with ImageJ software (ver. 1.42q; National Institutes of Health, USA). The minor-to-major axis length was also estimated to compare the shapes of the neurons.

Spontaneous firing activity was recorded in the cell-attached voltage-clamp mode. The frequency of spontaneous firing rate and coefficient of variation (CV) of interspike interval (ISI) were measured from stable electrophysiological recordings lasting for 2 to 4.5 min (mean, 2.7 min) and for 32 to 791 action potentials (mean, 317). Neurons firing at less than 0.1 Hz were considered 'silent neurons' and excluded from analysis.

The types of the PVN neurons were determined under whole-cell current-clamp mode by applying a series of progressively depolarizing pulses of 250 msec after a hyperpolarizing pulse of 250 msec to hyperpolarize the neuron to around  $-100$  mV [18,22]. A segment of membrane voltages (for 100 msec) was also digitized before and after each test pulse (Table 1) [18]. All labeled neurons were identified as type II, showing a pronounced dampening of the membrane charging curve and onset of the first action potential with little delay in response to the current protocol. After the cell type was determined, spontaneous action potentials ( $\sim 2$  min) were recorded, and the postsynaptic synaptic currents were recorded

under voltage-clamp mode.

### Data analysis

The mean frequency of neuron firing activity was analyzed by using the Mini Analysis Program (ver. 6.0; Synaptosoft, USA), excluding those neurons displaying a mean frequency of  $< 0.1$  Hz. The CV of ISIs was determined by dividing the SD of the ISIs by the mean ISI. The resting membrane potential (RMP) was measured from stable segment voltage records obtained between spontaneous action potentials. For the analysis of the action potential parameters, well selected spontaneous action potential events were analyzed by using the Mini Analysis Program as described earlier [17]. Briefly, the 10% to 90% rise time, 37% to 90% decay time, half-action potential duration, amplitude, threshold, and after-hyperpolarization measures were obtained by using the threshold as the baseline. The RMP and threshold were presented after correcting the liquid junction potential;  $-14.3$  mV for the data recorded with the pipettes filled K-gluconate-rich solution and  $-4.3$  mV for the data recorded with the pipette filled with the KCl-rich pipette solution.

For the 10% to 90% rise time and the 37% to 90% decay time of postsynaptic currents, the constants were obtained from the best-fit ( $R^2 \geq 0.9999$ ) parameters with a built-in double-exponential equation. The weighted time constant was obtained by using the Mini Analysis Program and was defined as  $\tau_w = (A_1\tau_1 + A_2\tau_2)/(A_1 + A_2)$ , where  $A_1$  and  $\tau_1$  are the amplitude and the time constant of the fast component and  $A_2$  and  $\tau_2$  are the amplitude and the time constant of the slow component at the 37% to 90% decay time.

All experimental values are expressed as the mean  $\pm$  SEM. The unpaired Student's *t*-test was used to assess the difference in the percentages of responding cells between the two groups. Fisher's exact test was used to evaluate the significance of differences in patterns of neuronal properties between various conditions. *P* values  $< 0.05$  were considered to indicate statistical significance.

**Table 1.** Membrane properties of PVN<sub>RVL</sub>M and PVN<sub>IML</sub> neurons

	PVN <sub>RVL</sub> M	PVN <sub>IML</sub>	<i>p</i> value
RMP (mV)	$-56.5 \pm 1.0$ (11)*	$-60.4 \pm 1.0$ (10)*	0.012
R <sub>in</sub> (M $\Omega$ )	$395 \pm 31$ (23)	$362.58 \pm 35$ (23)	0.488
$\tau_m$ (msec)	$26.0 \pm 2.9$ (23)	$25.2 \pm 4.1$ (23)	0.877
C <sub>m</sub> (pF)	$66.9 \pm 5.6$ (23)	$67.2 \pm 5.7$ (23)	0.965
Area (cm <sup>2</sup> )	$5.55 \pm 0.2$ (43)	$5.77 \pm 0.2$ (33)	0.44
Round	$0.61 \pm 0.02$ (43)	$0.55 \pm 0.02$ (33)	0.09

Data are presented as mean  $\pm$  SEM. The number of the cells tested in each group is given in parentheses. PVN, paraventricular nucleus; RVL, rostral ventrolateral medulla; IML, intermediolateral horn of the spinal cord; RMP, resting membrane potential; R<sub>in</sub>, input resistance;  $\tau_m$ , membrane time constant; C<sub>m</sub>, membrane capacitance. \**p*  $< 0.05$ .

## Results

The results in the present study are based on electrophysiological recordings obtained from a total of 117 labeled pre-sympathetic neurons (63 PVN<sub>RVL</sub>M and 54 PVN<sub>IML</sub> neurons) that were located in the dorsal and ventral subdivisions of the PVN (panel A in Supplementary Fig. 1). Table 1 presents a summary of the basic membrane properties of the two neuron groups recorded under pipettes filled with K-gluconate-rich pipette solution. The RMP of PVN<sub>RVL</sub>M was more depolarized, by about 4 mV, than that of PVN<sub>IML</sub> neurons (*p*  $< 0.05$ ). The other three parameters (input resistance, membrane capacitance, and time constant) were not different between the two neuron groups. The mean neuron sizes of the two groups, estimated

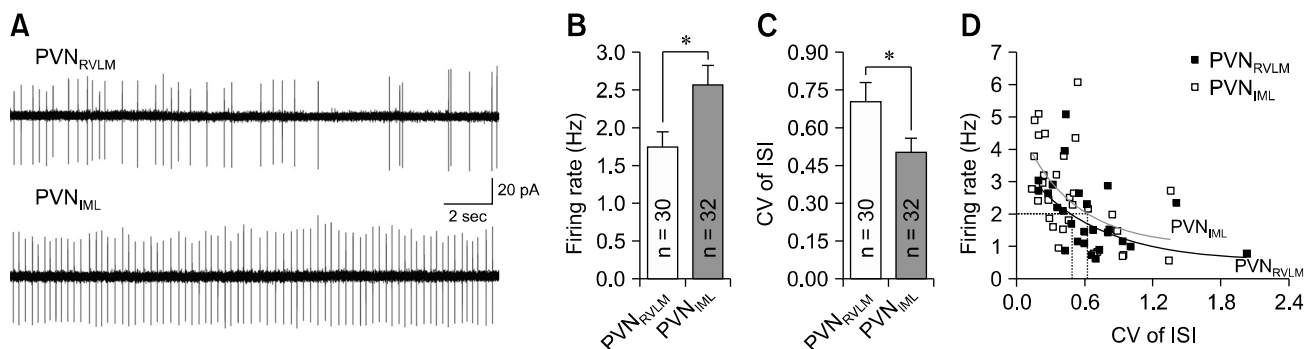


**Fig. 1.** The firing activity in PVN<sub>RVLM</sub> and PVN<sub>IML</sub> neurons. (A) Representative traces showing spontaneous firing activities of a PVN<sub>RVLM</sub> neuron and a PVN<sub>IML</sub> neuron. (B and C) Cumulative bar graphs showing the mean frequency of spontaneous spikes (B) and the coefficient of variance (CV) of the interspike interval (ISI) in PVN<sub>RVLM</sub> and PVN<sub>IML</sub> neurons (C). (D) Plot of firing rate vs. the CV of the ISI. The curves were drawn by fitting the data with the equation  $y = a + b \times x^c$ . The CV values in the PVN<sub>IML</sub> neurons tended to be smaller than those in the PVN<sub>RVLM</sub> neurons at the same firing rate. The values in the bars (B and C) represent the total number of neurons tested. Values represent mean  $\pm$  SEM. Asterisks indicate  $p < 0.05$  obtained by the unpaired Student's *t*-test. PVN, paraventricular nucleus; RVLM, rostral ventrolateral medulla; IML, intermediolateral horn of the spinal cord.

from the area of PC monitor images, were not significantly different ( $5.55$  vs.  $5.77$  cm<sup>2</sup>;  $p = 0.44$ ). Moreover, the two neuron groups did not differ in their minor-to-major axis ratios, an estimate of the ovality of the cells ( $0.61$  vs.  $0.55$ ;  $p = 0.09$ ).

### Spontaneous firing activity

In the cell-attached mode, 62 of the 80 neurons tested (77.5%) spontaneously fired (43 PVN<sub>RVLM</sub> neurons and 37 PVN<sub>IML</sub> neurons). The proportions of spontaneously active and silent neurons were not significantly different between the PVN<sub>RVLM</sub> and PVN<sub>IML</sub> neurons (70% vs. 86%;  $p > 0.05$ , Fisher exact test). Panel A in Fig. 1 illustrates representative traces showing spontaneous tonic irregular (PVN<sub>RVLM</sub>) and regular (PVN<sub>IML</sub>) firing activities in a PVN<sub>RVLM</sub> neuron with a frequency of 1.75 Hz (CV = 0.93) and in a PVN<sub>IML</sub> neuron with a frequency of 3.65 Hz (CV = 0.14). The mean frequency of the spontaneous firing activity of the PVN<sub>IML</sub> neurons ( $2.57 \pm 0.26$  Hz [ $n = 32$ ]) was significantly higher than that of the PVN<sub>RVLM</sub> neurons ( $1.74 \pm 0.21$  Hz [ $n = 30$ ]) ( $p < 0.05$ ; panel B in Fig. 1). The overall CV of the inter-event interval for spontaneous firing was significantly lower in the PVN<sub>IML</sub> neurons ( $0.50 \pm 0.06$  [ $n = 32$ ]) than in the PVN<sub>RVLM</sub> neurons ( $0.70 \pm 0.08$  [ $n = 30$ ]) ( $p < 0.05$ ; panel C in Fig. 1). The CV values tended to be smaller in the PVN<sub>IML</sub> neurons than in the PVN<sub>RVLM</sub> neurons at the same frequency. As marked by a dotted line (panel D in Fig. 1), the CV of the ISI was smaller in the PVN<sub>IML</sub> neurons than in the PVN<sub>RVLM</sub> neurons at 2 Hz ( $0.48$  vs.  $0.62$ ). These results indicate that the baseline firing activity of the PVN<sub>RVLM</sub> neurons was lower and that their firing pattern was more irregular than those of the PVN<sub>IML</sub> neurons.

### Spontaneous action potential

We further compared the properties of spontaneous action

potentials recorded in whole-cell current-clamp mode (Fig. 2). The neurons of the two groups also fired spontaneously under the whole-cell mode, and the firing frequency was slightly larger than those recorded in the cell-attached mode. Under these experimental conditions, the firing rates were not significantly different between the two neuron groups, but the value in the PVN<sub>IML</sub> neurons was greater. This trend was consistent with that of the spontaneous action potentials in cell-attached mode (PVN<sub>RVLM</sub>, 2.17 Hz vs. PVN<sub>IML</sub>, 2.91 Hz;  $p > 0.05$ ).

As shown in Fig. 2, the two neuron groups differed in their spontaneous action potential properties. Panel A in Fig. 2 illustrates representative spontaneous action potentials from PVN<sub>RVLM</sub> (RMP,  $-56.07$  mV; threshold,  $-43.09$  mV; rise time, 0.95 msec; decay time, 1.05 msec; half-APD [duration of action potential at half amplitude], 2.15 msec) and PVN<sub>IML</sub> (RMP,  $-60.53$  mV; threshold,  $-39.93$  mV; rise time, 0.6 msec; decay time, 0.75 msec; half-APD, 1.65 msec) neurons, respectively. The 10% to 90% rise time, 37% to 90% decay time and half-APD are significantly larger in PVN<sub>RVLM</sub> neurons than in PVN<sub>IML</sub> neurons (panels B–D in Fig. 2). The amplitude (PVN<sub>RVLM</sub>,  $62.78 \pm 3.37$  mV [ $n = 11$ ] vs. PVN<sub>IML</sub>,  $65.59 \pm 3.18$  mV [ $n = 10$ ];  $p > 0.05$ ), threshold (PVN<sub>RVLM</sub>,  $-42.12 \pm 0.82$  mV [ $n = 11$ ] vs. PVN<sub>IML</sub>,  $-44.90 \pm 1.82$  mV [ $n = 10$ ];  $p > 0.05$ ), and the peaks of the after-hyperpolarization potential (PVN<sub>RVLM</sub>,  $21.98 \pm 1.26$  mV [ $n = 11$ ] vs. PVN<sub>IML</sub>,  $25.02 \pm 2.22$  mV [ $n = 10$ ];  $p > 0.05$ ) were not significantly different.

### Miniature postsynaptic current

To examine, in detail, the properties of the synaptic currents in the two neuron groups, we analyzed the miniature postsynaptic currents of the pre-sympathetic neurons recorded under whole-cell mode. mIPSCs were recorded with the pipette

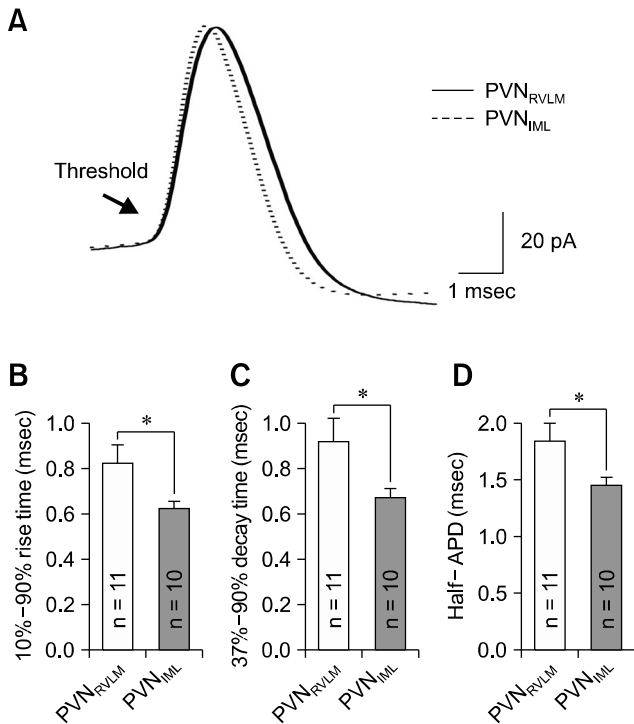


**Fig. 2.** The parameters of spontaneous action potentials in PVN<sub>RVLM</sub> and PVN<sub>IML</sub> neurons. (A) Representative action potentials from a PVN<sub>RVLM</sub> neuron (solid line; RMP, -56.07 mV; threshold, -43.09 mV; rise time, 0.95 msec; decay time, 1.05 msec; half-APD, 2.15 msec) and a PVN<sub>IML</sub> neuron (dotted line; RMP, -60.53 mV; threshold, -39.93 mV; rise time, 0.6 msec; decay time, 0.75 msec; half-APD, 1.65 msec) were overlapped at threshold. Cumulative bar graphs showing the 10% to 90% rise time (B), 37% to 90% decay time (C) and half-APD (D) in PVN<sub>RVLM</sub> and PVN<sub>IML</sub> neurons. The values in the bars (B-D) represent the total number of neurons tested. Values represent mean ± SEM. Asterisks indicate *p* < 0.05 by the unpaired Student's *t*-test. PVN, paraventricular nucleus; RVLM, rostral ventrolateral medulla; IML, intermediolateral horn of the spinal cord; half-APD, duration of action potential at half amplitude.

filled with the KCl-rich solution in the presence of tetrodotoxin (TTX, a Na<sup>+</sup> channel blocker that blocks spontaneous action potentials), CNQX, and AP5 (blockers of EPSC) at a holding potential of -70 mV (junction potential, -4.3 mV). Panels A and B in Fig. 3 show representative traces of mIPSCs in the PVN<sub>RVLM</sub> and PVN<sub>IML</sub> neurons, respectively. There were markedly more numerous synaptic events in the PVN<sub>RVLM</sub> neurons than in the PVN<sub>IML</sub> neurons. The frequency of mIPSCs in the PVN<sub>RVLM</sub> neurons (3.17 ± 0.67 Hz [n = 20]) was higher than the corresponding frequency in the PVN<sub>IML</sub> neurons (1.53 ± 0.23 Hz [n = 17]) (*p* < 0.05; panel C in Fig. 3). However, the mean amplitude was not significantly different between the two neuron groups (65.7 ± 7.05 pA vs. 59.2 ± 6.41 pA; *p* = 0.51) (panel D in Fig. 3). Overall, the spontaneous inhibitory inputs in

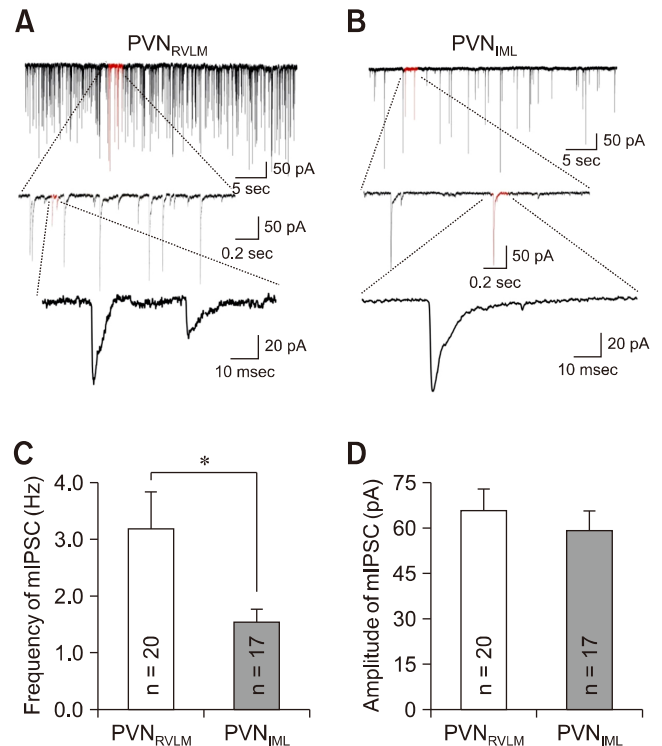


**Fig. 3.** Miniature inhibitory postsynaptic current (mIPSC) in PVN<sub>RVLM</sub> and PVN<sub>IML</sub> neurons. Representative current traces of mIPSCs in a PVN<sub>RVLM</sub> neuron (A) and a PVN<sub>IML</sub> neuron (B) (*V<sub>h</sub>* = -70 mV). Cumulative bar graphs showing the mean frequency (C) and mean amplitude (D) of the mIPSCs. The values in the bars (C and D) represent the total numbers of neurons tested. Values are mean ± SEM. Asterisk indicates *p* < 0.05 by the unpaired Student's *t*-test. PVN, paraventricular nucleus; RVLM, rostral ventrolateral medulla; IML, intermediolateral horn of the spinal cord.

the PVN<sub>RVLM</sub> neurons were about twice as strong as those in the PVN<sub>IML</sub> neurons, which likely explains the lower baseline firing activity of the PVN<sub>RVLM</sub> neurons.

We further determined the rise and decay times of mIPSCs by fitting the data points with a double-exponential equation, as described in the Materials and Methods section (panel A in Fig. 4). The mIPSCs of the RVLM neurons peaked earlier than those of the PVN<sub>IML</sub> neurons. The rise time of the mIPSCs in the PVN<sub>RVLM</sub> neurons (0.76 ± 0.05 msec [n = 18]) was shorter than that of the PVN<sub>IML</sub> neurons (0.95 ± 0.04 msec [n = 17]) (*p* < 0.05; panel B in Fig. 4). In contrast, the weighted decay times of the mIPSCs were not significantly different between the PVN<sub>RVLM</sub> and the PVN<sub>IML</sub> neurons (9.92 ± 0.50 [n = 18] vs. 11.17 ± 0.69 msec [n = 17]; *p* > 0.05) (panel C in Fig. 4).

We also recorded mEPSCs in the presence of TTX and bicuculline (GABA<sub>A</sub> receptor blocker) with a recording pipette filled with K<sup>+</sup>-gluconate solution. In contrast to mIPSCs, there were no significant differences between the two neuron groups

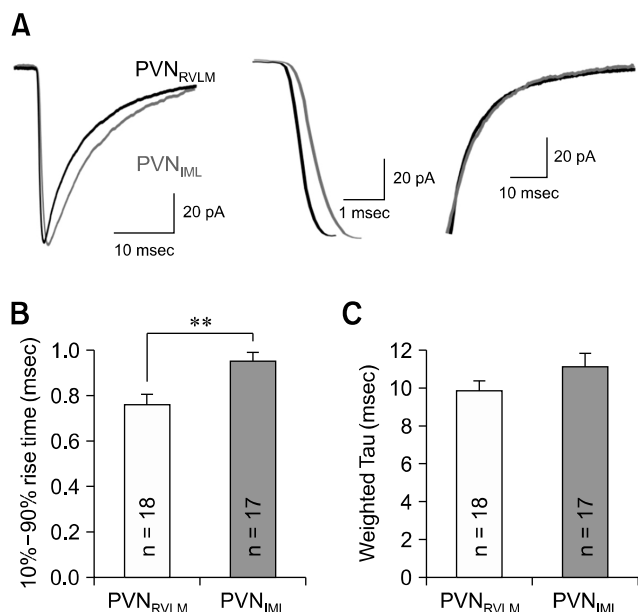


**Fig. 4.** The miniature inhibitory postsynaptic current (mIPSC) kinetics in the PVN<sub>RVLM</sub> and the PVN<sub>IML</sub> neurons. (A) Representative traces of mIPSCs in a PVN<sub>RVLM</sub> neuron (black) and a PVN<sub>IML</sub> neuron (gray) (left). Illustration of the 10% to 90% rise time and the decay time at an expanded time scale (middle and right). (B) Summary bar graphs showing the mean 10% to 90% rise time in the PVN<sub>RVLM</sub> and PVN<sub>IML</sub> neurons. (C) Summary bar graphs displaying the weighted decay time constant under a well-fitted second exponential. The values in the bars (B and C) represent the total numbers of neurons tested. Values are mean  $\pm$  SEM. Double asterisk indicates  $p < 0.05$  by the unpaired Student's *t*-test. PVN, paraventricular nucleus; RVLM, rostral ventrolateral medulla; IML, intermediolateral horn of the spinal cord.

in the frequency (PVN<sub>RVLM</sub>,  $3.85 \pm 0.50$  Hz [ $n = 13$ ] vs. PVN<sub>IML</sub>,  $5.10 \pm 0.63$  Hz [ $n = 14$ ];  $p > 0.05$ ) or amplitude (PVN<sub>RVLM</sub>,  $20.4 \pm 1.51$  pA [ $n = 13$ ] vs. PVN<sub>IML</sub>,  $25.5 \pm 3.08$  pA [ $n = 14$ ];  $p > 0.05$ ) of the mEPSCs. No significant differences were found in the rise time (PVN<sub>RVLM</sub>,  $0.68 \pm 0.05$  msec [ $n = 12$ ] vs. PVN<sub>IML</sub>,  $0.74 \pm 0.06$  msec [ $n = 14$ ];  $p > 0.05$ ) or the weighted decay time constant (PVN<sub>RVLM</sub>,  $3.36 \pm 0.26$  msec [ $n = 12$ ] vs. PVN<sub>IML</sub>,  $3.17 \pm 0.30$  msec [ $n = 14$ ];  $p > 0.05$ ) between the two neuron groups.

## Discussion

In the present study, we observed that two pre-sympathetic neuron groups, located and intermingled within the dorsal and ventral subdivisions of the PVN, are different in their baseline electrophysiological properties. When compared to the PVN<sub>IML</sub> neurons, the PVN<sub>RVLM</sub> neurons showed 1) more depolarized RMP, 2) lower baseline firing activity with more irregular intervals, 3) slower rise and decay and longer duration of spontaneous action potentials, and 4) greater frequency and rise

time of GABAergic mIPSC. These results newly reveal that intrinsic membrane properties such as RMP and the action potential parameters are significantly different between the two neuron groups. The study also confirms our previous results of lower baseline firing activity and greater inhibitory synaptic activity in PVN<sub>RVLM</sub> neurons.

The baseline firing rate of the PVN<sub>RVLM</sub> neurons recorded in the cell-attached mode is lower than that of the PVN<sub>IML</sub> neurons (1.74 vs. 2.57 Hz). This is in close agreement with the results in our previous report ([18]; 1.79 vs. 3.26 Hz), in which the firing activities of two pre-sympathetic neuron groups were observed under similar experimental conditions. Although the number of reports on the firing rate of pre-sympathetic PVN neurons recorded in cell-attached mode is limited, the results of the present study confirm the results of our previous report. This observation remains to be further examined by other laboratories in the future.

The most salient results of this study are that the RMPs and properties of spontaneous action potentials are different in the two neuron types ( $p < 0.05$ ). As for the RMP (PVN<sub>RVLM</sub> vs. PVN<sub>IML</sub>,  $-56.5$  vs.  $60.4$  mV;  $p < 0.05$ ), the result of this study is different from that in the previous report in which the RMPs were not different between two pre-sympathetic neuron groups ( $62.1$  vs.  $61.8$  mV; [18]). This discrepancy could be due to the differences in measuring the RMP. In the present study, the RMP of a neuron was obtained by averaging the membrane potentials in the stable segments of different time points ( $\sim 10$ ) in the voltage record, whereas, in our previous study [18], the RMP was measured from voltage responses ( $\sim 100$  msec) to the current pulses to determine the cell type. In the latter case, the membrane potential was measured in segments of voltage records with highly fluctuating spontaneous action potentials because the test pulses, once initiated, are delivered all at once as designed by the pClamp program. Considering the differences in membrane potential measurement, it is likely that the membrane potential values in this study are measured more accurately, and hence, the two neuron types are different in their RMP. This discrepancy remains to be studied further.

To our knowledge, this study is the first to show that the properties of spontaneous action potentials are different between two pre-sympathetic neuron groups in the PVN. The rise and decay times and duration of spontaneous action potentials are greater in the PVN<sub>RVLM</sub> neurons than in the PVN<sub>IML</sub> neurons. The PVN<sub>RVLM</sub> neurons showed lower baseline firing activity and more irregular firing pattern than the PVN<sub>IML</sub> neurons. Considering that an action potential fires when the membrane potential crosses the threshold, the firing frequency and ISIs in a neuron depend on the intrinsic membrane properties as well as extrinsic properties [1]. In the present study, the RMP of PVN<sub>RVLM</sub> neurons is about 4 mV more depolarized, and the spontaneous action potentials of PVN<sub>RVLM</sub> neurons had longer kinetics (rise time, decay time, and duration,

$p < 0.05$ ) than those of the PVN<sub>IML</sub> neurons. It is well known that the rise time of the action potential is slowed when the number of active Na<sup>+</sup> channels is reduced [19]. The sodium channel will lose excitability when inactivated by depolarizing pre-pulses [16]. Therefore, it is likely that the larger rise time in action potential of the PVN<sub>RVL</sub>M neurons is due to the inactivation of some Na<sup>+</sup> channels at a depolarized RMP. Alternatively, the lower density of Na<sup>+</sup> channels in the axon initial segment in a neuron can also increase the action potential rise time as reported previously [21]. Further study is needed to confirm the Na<sup>+</sup> channel mechanisms underlying the differences in the rise times of two pre-sympathetic PVN neuron groups.

In the regulation of action potential duration and decay time, the voltage-activated potassium channels (Kv3.1–3.2) have a critical role in modeling the action potential repolarization phase. Blockade of Kv3.1–3.2 channels with tetraethylammonium prolongs the decay time and decreases the firing rate in response to current inputs [13]. Multiple Ca<sup>2+</sup> channels are also largely involved in determining firing rates and action potential shapes, especially the repolarization phase. For example, Ca<sup>2+</sup><sub>v1.1</sub> channels are associated with other Ca<sup>2+</sup> channel subtypes [3] to shape action potential repolarization, or in medial vestibular neurons to decrease the firing rate under Ca<sup>2+</sup> influx [27]. Taken together, the greater rise time and decay time of the action potentials in the PVN<sub>RVL</sub>M neurons suggests a lower density or activity of voltage-dependent Na<sup>+</sup> channels but a greater expression or activity of multiple types of calcium channels and the potassium channel in the PVN<sub>RVL</sub>M neurons than in the PVN<sub>IML</sub> neurons. These differences are also likely to be one of the mechanisms underlying the lower baseline firing activity seen in the PVN<sub>RVL</sub>M neurons.

In addition to the intrinsic property effect, extrinsic inputs can also affect the firing rate [1]. The frequency of mIPSCs in this study was significantly higher in the PVN<sub>RVL</sub>M neurons than in the PVN<sub>IML</sub> neurons, and the rise time of the mIPSCs was shorter. In the PVN neurons, GABA can induce a tonic current as well as phasic IPSCs [24]. Although we did not compare the GABA<sub>A</sub> receptor-mediated tonic current, it is likely that the GABAergic tonic current is also greater in PVN<sub>RVL</sub>M neurons because the tonic current is activated by GABA spillover from the synaptic cleft [14]. The observation that the PVN<sub>RVL</sub>M neurons had a greater mIPSC frequency suggests that there are more synaptic contacts per neuron in PVN<sub>RVL</sub>M neurons than in PVN<sub>IML</sub> neurons. The observation that the rise time of the mIPSCs in PVN<sub>RVL</sub>M neurons was shorter than in the PVN<sub>IML</sub> neurons could have been due to these differences in the synaptic cleft. For example, Salin and Prince [29] reported that the rise time of mIPSCs was increased by 19% and 26% following an increase in the distance of the recording cells from the points of drug application from 100 to 150  $\mu$ m to 180 to 330  $\mu$ m. Differences in the GABA<sub>A</sub> receptor subunit composition are

another possible mechanism for the faster rise of mIPSCs in the PVN<sub>RVL</sub>M neurons [33]. GABAergic events mediated by  $\alpha_2\beta_3\delta_2$  receptors were found to be faster (rise time,  $\sim 2$  msec) than those mediated by  $\alpha_6\beta_3\delta$  receptors (rise time,  $\sim 20$  msec) in neuron-human embryonic kidney cell heterosynapses [37]. Further studies are needed to fully elucidate the detailed mechanisms underlying the differences observed in this study in the intrinsic and synaptic properties of these two neuron groups. Overall, our results suggest that the lower firing rate seen in the PVN<sub>RVL</sub>M neurons may have been due to the slower activation and longer duration of the action potentials, as well as to stronger inhibitory synaptic currents, whereas the more irregular firing pattern of PVN<sub>RVL</sub>M neurons is largely due to the more frequent inhibitory synaptic inputs. The results are similar to those reported for the synaptic mechanisms responsible for the altered firing rate and patterns in the interneurons of the rats with cortical dysplasia [39], and they help to indicate possible mechanisms for the elevated firing rate in the PVN<sub>RVL</sub>M neurons in heart failure rats [18].

Based on the difference in electrophysiological properties between PVN<sub>RVL</sub>M and PVN<sub>IML</sub> neurons, one may speculate the possible functions of these two neuron groups. Since PVN<sub>RVL</sub>M neurons receive more abundant GABAergic inhibitory synaptic inputs, these neurons are likely to play a more integrative role than PVN<sub>IML</sub> neurons. For example, PVN neurons receive GABAergic inputs from the ventrolateral preoptic, peri-PVN area, a series of subnuclei of the bed nucleus of the stria terminalis and dorsomedial hypothalamic area. These GABA cells transmit information from higher centers, such as the ventral subiculum, central amygdaloid nucleus, lateral septal nucleus, medial amygdaloid nucleus, and medial prefrontal cortex [11]. In addition, the observation that the two neuron groups had different patterns of baseline firing activity indicates that although they are located close to each other in the PVN, their functions are different. It has been reported that in response to fear stressors, PVN<sub>IML</sub> neurons were more activated than PVN<sub>RVL</sub>M neurons [5]. Taken together, these results indicate that PVN<sub>RVL</sub>M and PVN<sub>IML</sub> neurons are likely to play different roles in sympathetic regulation.

In interpreting the observations made in this study, one should keep in mind the following limitations. Firstly, the pre-sympathetic PVN neurons send descending fibers to the IML cell column of the thoraco-lumbar spinal cord, as well as to the region of the RVL, and approximately 30% of the spinally-projecting PVN neurons have collateral inputs to the RVL region [2,26]. Secondly, although the labeled pre-sympathetic neurons were found in both dorsal and ventral subdivisions, in the present study the neurons in the dorsal subdivision were selected more frequently for recording (82.4% in 17 PVN<sub>IML</sub>, and 68.2% in 22 PVN<sub>RVL</sub>M neurons; data not illustrated). At present, little has been reported about the functional differences between the pre-sympathetic neurons in

located in dorsal and ventral subdivisions in the PVN. Finally, the electrophysiological activities of neurons in slice preparations can be different from those recorded *in vivo* due to differences in neuronal connectivity and recording conditions. For example, the firing rate of PVN<sub>RVL</sub>M neurons was 2.6 Hz in rats [38], whereas that of PVN<sub>IML</sub> neurons was 2.7 Hz [9]; these values are different from the firing rates recorded *in vitro* in this and previous studies [18].

Taken together, our results indicate that the two pre-sympathetic neuron types in the PVN are different in intrinsic properties (RMP and action potential) as well as extrinsic inputs (GABAergic inhibitory synaptic inputs). The differences in baseline intrinsic and extrinsic electrophysiological properties may explain the lower excitability of the PVN<sub>RVL</sub>M neurons. In addition, the observation that the PVN<sub>RVL</sub>M neurons receive greater inhibitory synaptic inputs also suggests that the PVN<sub>RVL</sub>M neurons play more integrative roles than those of the PVN<sub>IML</sub> neurons. Our observations provide further experimental evidence that these two pre-sympathetic neuron groups play different roles in the regulation of the sympathetic nervous system in normal and disease states.

## Acknowledgments

This work was supported by the National Research Foundation of Korea (NRF), which is funded by the Ministry of Education, Science and Technology (2011-0025817 & 2016R1D1A3B03932241) and partially supported by the Research Institute for Veterinary Science at Seoul National University.

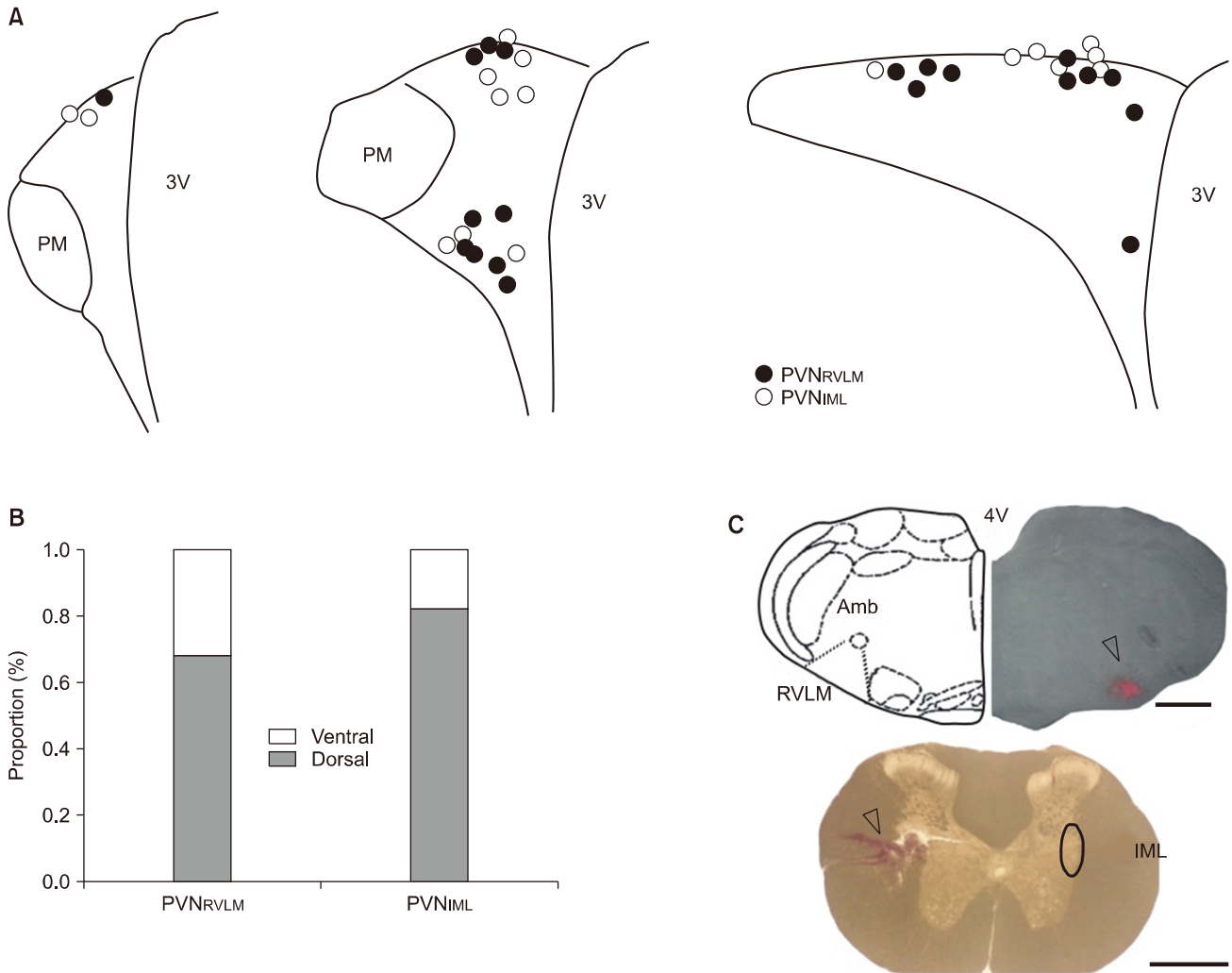
## Conflict of Interest

The authors declare no conflicts of interest.

## References

1. **Abbott LF, Fusi S, Miller KD.** Theoretical approaches to neuroscience: examples from single neurons to networks. In: Kandel ER, Schwartz JH, Jessell TM, Siegelbaum SA, Hudspeth AJ, Mack S (eds.). *Principles of Neural Science*. 5th ed. pp. 1601-1617, McGraw-Hill Professional Publishing, New York, 2012.
2. **Badoer E.** Hypothalamic paraventricular nucleus and cardiovascular regulation. *Clin Exp Pharmacol Physiol* 2001, **28**, 95-99.
3. **Berkefeld H, Fakler B.** Repolarizing responses of BK<sub>Ca</sub>-Cav complexes are distinctly shaped by their Cav subunits. *J Neurosci* 2008, **28**, 8238-8245.
4. **Brown CH, Bains JS, Ludwig M, Stern JE.** Physiological regulation of magnocellular neurosecretory cell activity: integration of intrinsic, local and afferent mechanisms. *J Neuroendocrinol* 2013, **25**, 678-710.
5. **Carive P, Gorissen M.** Premotor sympathetic neurons of conditioned fear in the rat. *Eur J Neurosci* 2008, **28**, 428-446.
6. **Cechetto DF, Saper CB.** Neurochemical organization of the hypothalamic projection to the spinal cord in the rat. *J Comp Neurol* 1988, **272**, 579-604.
7. **Cham JL, Badoer E.** Exposure to a hot environment can activate rostral ventrolateral medulla-projecting neurons in the hypothalamic paraventricular nucleus in conscious rats. *Exp Physiol* 2008, **93**, 64-74.
8. **Cham JL, Klein R, Owens NC, Mathai M, McKinley M, Badoer E.** Activation of spinally projecting and nitergic neurons in the PVN following heat exposure. *Am J Physiol Regul Integr Comp Physiol* 2006, **291**, R91-101.
9. **Chen QH, Toney GM.** Identification and characterization of two functionally distinct groups of spinal cord-projecting paraventricular nucleus neurons with sympathetic-related activity. *Neuroscience* 2003, **118**, 797-807.
10. **Coote JH.** A role for the paraventricular nucleus of the hypothalamus in the autonomic control of heart and kidney. *Exp Physiol* 2005, **90**, 169-173.
11. **Cullinan WE, Ziegler DR, Herman JP.** Functional role of local GABAergic influences on the HPA axis. *Brain Struct Funct* 2008, **213**, 63-72.
12. **Engelmann M, Landgraf R, Wotjak CT.** The hypothalamic-neurohypophysial system regulates the hypothalamic-pituitary-adrenal axis under stress: an old concept revisited. *Front Neuroendocrinol* 2004, **25**, 132-149.
13. **Erisir A, Lau D, Rudy B, Leonard CS.** Function of specific K<sup>+</sup> channels in sustained high-frequency firing of fast-spiking neocortical interneurons. *J Neurophysiol* 1999, **82**, 2476-2489.
14. **Farrant M, Nusser Z.** Variations on an inhibitory theme: phasic and tonic activation of GABA<sub>A</sub> receptors. *Nat Rev Neurosci* 2005, **6**, 215-229.
15. **Hallbeck M, Larhammar D, Blomqvist A.** Neuropeptide expression in rat paraventricular hypothalamic neurons that project to the spinal cord. *J Comp Neurol* 2001, **433**, 222-238.
16. **Hammond C.** The voltage-gated channels of Na<sup>+</sup> action potentials: generalization. In: Hammond C (ed.). *Cellular and Molecular Neurophysiology*. 3rd ed. pp. 45-82, Academic Press, San Diego, 2008.
17. **Han SK, Chong W, Li LH, Lee IS, Murase K, Ryu PD.** Noradrenaline excites and inhibits GABAergic transmission in parvocellular neurons of rat hypothalamic paraventricular nucleus. *J Neurophysiol* 2002, **87**, 2287-2296.
18. **Han TH, Lee K, Park JB, Ahn D, Park JH, Kim DY, Stern JE, Lee SY, Ryu PD.** Reduction in synaptic GABA release contributes to target-selective elevation of PVN neuronal activity in rats with myocardial infarction. *Am J Physiol Regul Integr Comp Physiol* 2010, **299**, R129-139.
19. **Hodgkin AL, Huxley AF.** A quantitative description of membrane current and its application to conduction and excitation in nerve. *J Physiol* 1952, **117**, 500-544.
20. **Jansen AS, Wessendorf MW, Loewy AD.** Transneuronal labeling of CNS neuropeptide and monoamine neurons after pseudorabies virus injections into the stellate ganglion. *Brain Res* 1995, **683**, 1-24.

21. **Kole MH, Ilshner SU, Kampa BM, Williams SR, Ruben PC, Stuart GJ.** Action potential generation requires a high sodium channel density in the axon initial segment. *Nat Neurosci* 2008, **11**, 178-186.
22. **Luther JA, Tasker JG.** Voltage-gated currents distinguish parvocellular from magnocellular neurones in the rat hypothalamic paraventricular nucleus. *J Physiol* 2000, **523**, 193-209.
23. **Palkovits M.** Interconnections between the neuroendocrine hypothalamus and the central autonomic system: Geoffrey Harris Memorial Lecture, Kitakyushu, Japan, October 1998. *Front Neuroendocrinol* 1999, **20**, 270-295.
24. **Pandit S, Jo JY, Lee SU, Lee YJ, Lee SY, Ryu PD, Lee JU, Kim HW, Jeon BH, Park JB.** Enhanced astroglial GABA uptake attenuates tonic GABA<sub>A</sub> inhibition of the presympathetic hypothalamic paraventricular nucleus neurons in heart failure. *J Neurophysiol* 2015, **114**, 914-926.
25. **Paxinos G, Watson C.** *The Rat Brain in Stereotaxic Coordinates*. 2nd ed. Academic Press, San Diego, 1986.
26. **Pyner S, Coote JH.** Identification of branching paraventricular neurons of the hypothalamus that project to the rostroventrolateral medulla and spinal cord. *Neuroscience* 2000, **100**, 549-556.
27. **Rehak R, Bartoletti TM, Engbers JD, Berecki G, Turner RW, Zamponi GW.** Low voltage activation of KCa<sub>v</sub>1.1 current by Cav3-KCa<sub>v</sub>1.1 complexes. *PLoS One* 2013, **8**, e61844.
28. **Renaud LP, Bourque CW.** Neurophysiology and neuropharmacology of hypothalamic magnocellular neurons secreting vasopressin and oxytocin. *Prog Neurobiol* 1991, **36**, 131-169.
29. **Salin PA, Prince DA.** Spontaneous GABA<sub>A</sub> receptor-mediated inhibitory currents in adult rat somatosensory cortex. *J Neurophysiol* 1996, **75**, 1573-1588.
30. **Saper CB.** Central autonomic system. In: Paxinos G (ed.). *The Rat Nervous System*. 3rd ed. pp. 761-796, Elsevier, San Diego, 2004.
31. **Sawchenko PE, Brown ER, Chan RK, Ericsson A, Li HY, Roland BL, Kovács KJ.** The paraventricular nucleus of the hypothalamus and the functional neuroanatomy of visceromotor responses to stress. *Prog Brain Res* 1996, **107**, 201-222.
32. **Sawchenko PE, Li HY, Ericsson A.** Circuits and mechanisms governing hypothalamic responses to stress: a tale of two paradigms. *Prog Brain Res* 2000, **122**, 61-78.
33. **Schofield PR, Darlison MG, Fujita N, Burt DR, Stephenson FA, Rodriguez H, Rhee LM, Ramachandran J, Reale V, Glencorse TA, Seeburg PH, Bamard EA.** Sequence and functional expression of the GABA<sub>A</sub> receptor shows a ligand-gated receptor super-family. *Nature* 1987, **328**, 221-227.
34. **Stern JE.** Electrophysiological and morphological properties of pre-autonomic neurones in the rat hypothalamic paraventricular nucleus. *J Physiol* 2001, **537**, 161-177.
35. **Swanson LW, Sawchenko PE.** Hypothalamic integration: organization of the paraventricular and supraoptic nuclei. *Annu Rev Neurosci* 1983, **6**, 269-324.
36. **Swanson LW, Sawchenko PE.** Paraventricular nucleus: a site for the integration of neuroendocrine and autonomic mechanisms. *Neuroendocrinology* 1980, **31**, 410-417.
37. **Wu X, Wu Z, Ning G, Guo Y, Ali R, Macdonald RL, De Blas AL, Luscher B, Chen G.**  $\gamma$ -Aminobutyric acid type A (GABA<sub>A</sub>) receptor  $\alpha$  subunits play a direct role in synaptic versus extrasynaptic targeting. *J Biol Chem* 2012, **287**, 27417-27430.
38. **Xu B, Zheng H, Patel KP.** Enhanced activation of RVLM-projecting PVN neurons in rats with chronic heart failure. *Am J Physiol Heart Circ Physiol* 2012, **302**, H1700-1711.
39. **Zhou FW, Roper SN.** Altered firing rates and patterns in interneurons in experimental cortical dysplasia. *Cereb Cortex* 2011, **21**, 1645-1658.



**Supplementary Fig. 1.** Distribution of the PVN neurons projecting to RVLM and IML. (A) Note that the neurons of both groups were found intermingled in the dorsal and ventral subdivisions of the PVN. A illustrates the location of neurons recorded from the slices of the anterior (left) to the posterior part of the PVN (right). (B) The bar graph summarizes the proportions of PVN<sub>RVLM</sub> and PVN<sub>IML</sub> neurons in the dorsal and ventral subdivisions. (C) Representative photographs showing sites of the FluoSphere injection, at a section (bregma -12 mm) including the RVLM (top) and the intermediolateral horn (IML) of spinal cord (T2; bottom). Scale bars = 1 mm. PVN, paraventricular nucleus; RVLM, rostral ventrolateral medulla; IML, intermediolateral horn of the spinal cord; 3V, the third ventricle; PM, posterior magnocellular; 4V, the fourth ventricle; Amb, the nucleus ambiguus.